Chemical Engineering Journal 149 (2009) 132–142

Contents lists available at ScienceDirect

Chemical Engineering Journal

journal homepage: www.elsevier.com/locate/cej

Development of a predictive mathematical model for coupled stokes/Darcy flows in cross-flow membrane filtration

N.S. Hanspal [a,*], A.N. Waghode [b], V. Nassehi [c], R.J. Wakeman [c]

[a] *Energy, Environment and Climate Change Group, School of Mechanical, Aerospace and Civil Engineering, University of Manchester (UMIST), Manchester, Lancashire M601QD, UK*
[b] *Halliburton KBR, Hill Park Court, Spring Field Drive, Leatherhead, KT22 7NL, UK*
[c] *Advanced Separation Technologies Group, Chemical Engineering Department, Loughborough University, LE113TU, UK*

ARTICLE INFO

Article history:
Received 6 May 2008
Received in revised form 1 October 2008
Accepted 9 October 2008

Keywords:
Stokes flow
Darcy flow
Cross-flow filtration
Coupled flows
Finite element modelling

ABSTRACT

Free flow regimes accompanied by porous walls feature commonly in a variety of natural processes and industrial applications such as groundwater flows, packed beds, arterial blood flows and cross-flow and dead-end filtrations. Cross-flow microfiltration or ultrafiltration processes are generally employed in a range of industrial situations ranging from oil to medical applications. The coupled free/porous fluid transport phenomenon plays an equally important role along with the particle transport mechanisms concerning the separation efficiency of cross-flow membrane filtration. To provide a theoretical background for the experimental outcomes of cross-flow filtration, a mathematically sound model is desired which can reliably represent the interfacial boundary whilst maintaining the continuity of flow field variables across the interface between the free and porous flow regimes. Notwithstanding the numerous attempts reported in the literature, the development of a generic mathematical model for coupled flows has been prohibited by the complexities of interactions between the free and the porous flow systems. Henceforth, the aim of present work is to gain a better mathematical understanding of the interfacial phenomena encountered in coupled free and porous flow regimes applicable to cross-flow filtration systems. The free flow dynamics can be justifiably represented by the Stokes equation whereas the non-isothermal, non-inertial and incompressible flow in a low permeability porous medium can be handled by the Darcy equation. Solutions to the system of partial differential equations (PDEs) are obtained using the finite element method employing mixed interpolations for the primary field variables which are velocity and pressure. A nodal replacement scheme previously developed by the same authors has been effectively enforced as the boundary constraint at the free/porous interface for coupling the two physically different flow regimes in a single mathematical model. A series of computational experiments for permeability values of the porous medium ranging between 10^{-6} and 10^{-12} m^2 have been performed to examine the susceptibility of the developed model towards complex and irregular shaped geometries. Our results indicate that at high permeability values, the discrepancy in mass balance calculations is observed to be significant for a curved porous surface, which may be attributed to the inability of the Darcy equation to represent the flow dynamics in a highly permeable medium. At a low permeability, a very small amount of fluid permeated through the free/porous interface as most of the fluid leaves the domain through the free flow exit. The geometry and permeability of the free/porous interface are found to affect the amount of fluid passing through the porous medium significantly. All the numerical solutions that are presented have been theoretically validated for their accuracy by computing the overall mass continuity across the computational domains.

1. Introduction

The combination of free flow and flow through a porous medium exists in a variety of fluid processes occurring naturally or taking place in many industrial applications such as cross-flow and dead-end filtration, heterogeneous catalytic reactions, subsurface flows and solidification of metal alloys. Though the flow regimes present in these processes seem to be similar, the flow field characteristics are observed to vary mainly due to the nature of the interface separating the free and porous regimes. In some of the above mentioned processes, the free/porous interface is distinct and stationary whereas in others the interface is moving with the fluid. Cross-flow

* Corresponding author.
E-mail address: navraj.hanspal@manchester.ac.uk (N.S. Hanspal).

1385-8947/$ – see front matter © 2008 Published by Elsevier B.V.
doi:10.1016/j.cej.2008.10.012

Nomenclature

K_x	permeability of medium in x-direction
K_y	permeability of medium in y-direction
p	hydrostatic fluid pressure
v_x	velocity of fluid in x-direction
v_y	velocity of fluid in y-direction

Greek symbols

η	viscosity of fluid
ρ	density of fluid

filtration is an effective separation technology that finds application in a wide range of areas including water treatment systems, clean environment technologies, and energy production.

Cross-flow membrane filtration, frequently termed low shear-tangential filtration is used to clean fluids that are difficult to filter and to separate fine matter such as cells, proteins, enzymes and viruses. Unlike the normal pressure driven dead-end filtration, the fluid is pumped to flow tangentially over a porous boundary, layer or surface. A small part of the fluid penetrates through the porous boundary and the major amount flows out of the filtration assembly which is then re-circulated. During the initial period of filtration, the cross-flow of fluid provides sufficient shear to drive the particles deposited on the porous surface to avoid blockage of the pores.

A significant contribution to modelling of cross-flow microfiltration is by Belfort and Nagata [1] who emphasized the need for detailed understanding of the fluid dynamics to analyse the effects of concentration polarisation and membrane fouling. In a later article, Belfort [2] attempted modelling of multiphase flows of macromolecules and colloidal suspensions through cross-flow filtration membranes. Besides this, enormous work has been listed in the literature concerning modelling characterization along with classification of membrane cross-flow filtrations ([3]; Schmitz et al. [40]; [4]). Huang and Morrissey [5] carried out finite element simulations of fluid dynamics in cross-flow polysulphone membrane ultrafiltration module to predict the effects of concentration polarisation. Richardson and Nassehi [42] developed a Streamline Upwind Petrov Galerkin (SUPG) finite element scheme to model the free flow domains having curved porous boundaries with a specialised case of cross-flow membrane filtrations. Ripperger and Altmann [6] have discussed in detail the historical developments in the cross-flow filtration along with the mechanisms behind particle depositions on the membrane surface.

Many factors such as the flow Reynolds number, physical properties of the porous medium and rheological behaviour directly affect the flow behaviour of laminar free flow adjacent to porous walls. Berman [7] attempted a solution to the problem of two-dimensional laminar flow in channels having porous walls based on the assumption of uniform wall suction. On similar grounds, Yuan and Finkelstein [43] came up with the solution for axisymmetric channels. Both these solutions are reported to be valid at values of Reynolds number nearing one. Following this, most important experimental and theoretical works on this topic were based on the hypothesis that a uniform value of filtration velocity exists along the porous wall which requires either a variable trans-membrane pressure drop or a permeability that varies along the length of the porous wall [8,9]. Durlofski and Brady [13] proved the existence of similarity solutions for two-dimensional channel flows for all ranges of Reynolds numbers, which is not true conversely for axisymmetric flows. Chatterjee and Belfort [35] presented a detailed review of mathematical models dealing with laminar fluid flow in a porous channel with wall suction or injection. More recently, Oxarango et al. [10] developed a one-dimensional model to determine laminar flow of fluid in a porous channel with wall suction or injection based on the combinations of perturbation analysis and averaging techniques. The model was validated against a CFD code and it was found out that the flow properties such as inertia terms which affect the wall suction conditions were preserved.

The conservation of linear momentum for free flow through the channel is generally expressed by Cauchy's equation containing terms corresponding to viscous or convective transport. In the case of generalised Newtonian fluids, the Cauchy's stress tensor is considered to be a function of the instantaneous rate of strain and is independent of memory of deformation. In some highly viscous incompressible fluid flows, the Reynolds number is small enough to neglect the contribution to the flow by a convection mechanism and Cauchy's equations takes the form of Stokes equations for creeping flow.

The origin and the fundamentals behind the existence of the Darcy equation have been described in detail by Lage [37]. The validity of Darcy's equation in representing flow through porous media is widely accepted [21,44]. The validity of the Darcy equation is subjected to assumptions such as low Reynolds number and no fluid/porous media interaction. Darcy's law faces severe criticisms regarding the order of the differential equation and the corresponding inability to specify no-slip boundary conditions at solid walls and impose the standard mass continuity restrictions at porous and open fluid interfaces. In addition Darcy's law is only valid for the value of Reynolds number close to unity. To ameliorate these limitations, various researchers came forward with different modifications to the conventional Darcy equation.

The porous medium is a material consisting of a solid structure with an interconnected void and on the pore scale, i.e. microscopic scale, flow quantities such as velocity and pressure will be irregular [11]. In real time experiments, the flow quantities are measured as an average over area or volume occupied over a number of pores (macroscopic level). Although the Darcy equation could be derived by cumulative averaging of the free flow equations over each and every individual pore, the free and porous flow regimes differ considerably on a macroscopic scale of reference. These two distinct flow regimes are interconnected by a rigid interface or barrier and the continuity of the physical entities associated with both the regimes across the barrier remains the crucial issue to be assessed in modelling of combined flow phenomena.

The complexities of interactions underlying coupled free and porous flow regimes have prevented development of a general mathematical model and a robust solution procedure, which is independent of the nature and geometry of flow regimes and the separating interface. A generic mathematical model is requisite which can represent the individual free and porous flow behaviour along with accurate interpretation of the interfacial physics. In addition, the different orders of velocity differentials in the Stokes and the Darcy equations exacerbate the situations and make their straightforward linking impossible due to the incompatibility of the boundary constraints.

To ameliorate the situation, researchers have proposed two radically different approaches. The first approach soley supports the modifications to the original Darcy equations such as the well-known Brinkman equation which introduces viscous diffusion [45]. The velocity derivatives in the Brinkman equation are of identical order to that of the Stokes equation and enhance their conjugate solution without any interfacial constraints. However, the theoretical study by Lundgren [46] and Kim and Russell [12] confirmed the applicability of the Brinkman equations only for porous media having higher permeability values ranging above 10^{-7} m^2. In addition, the Brinkman equation introduces a term known as effec-

tive Brinkman viscosity, whose value unfortunately can neither be determined theoretically nor can be evaluated by experimentation [11,13]. Therefore, in most cases the Brinkman effective viscosity is assumed to be equal to the fluid viscosity [14,15]. However, in filtration of suspensions the effective viscosity of the feed stream cannot be equal to the clean filtered fluid viscosity and may lead to wrong interpretation of actual process. Secondly, in the case of porous media of very low permeability of the order of $10^{-12}\,m^2$ or greater, the possible occurrence of a boundary layer inside the porous medium in the vicinity of interface is almost impossible.

The second approach emphasizes the need for specification of some kind of slip condition at the interface relating the field variables such as velocity and pressure and in some cases stress from both the flow regimes. Beavers and Joseph (1967) [44] proposed that the interfacial velocities of the freely flowing fluid and the fluid velocity in the porous matrix could be related by an ad hoc matching interface boundary condition

$$\frac{\partial u_f}{\partial y} = \frac{\alpha}{\sqrt{K}}(u_f - u_m)$$

where u_f is the velocity of the flow in fluid calculated at $y = 0^+$ and u_m is the seepage velocity measured at small distance outside the interface, suggesting the existence of a thin layer just inside the porous medium over which the velocity transition occurs. The dimensionless slip wall coefficient α is independent of the fluid viscosity and apart from permeability depends on the structural parameters of the porous medium and is specific to the geometric features of the interface. Followed by Beavers and Joseph (1967) [44] many analogous relationships, modifications and alterations for this interfacial constraint have been proposed by Saffman [47], Jones [16], Neale and Nader [17], Haber and Mauri [48], Vafai and Thiyagaraja [15], Sahraoui and Kaviany [18] and Ochoa-Tapia and Whitaker [19].

The slip boundary conditions like the classic Beavers–Joseph constraints require continuation of the velocity and tangential components of shear stress. In this case, the interfacial velocities of the fluid in the free flow and porous regimes are related by an ad hoc matching condition, which admits a discontinuity in their tangential component. This is an empirical approach deduced from a simple one-dimensional situation and its extension to multi-dimensional scenarios is not well understood. The imposition of a slip boundary condition at the free/porous interface includes the calculation of a slip wall coefficient α. Though the actual prediction of this coefficient by any experimental or analytical technique appears to be straightforward for simplistic domains, its evaluation for irregular and complex geometrical computational domains is practically impossible.

A community of mathematicians and physicists have been working over the past three decades to find analytical and numerical solutions to the conjugate problem of Navier–Stokes and Darcy equations. The foundation of most of these solution techniques is on the application of Beavers–Joseph slip wall conditions at the free/porous interface. Salinger et al. [20] presented a numerical procedure to solve large scale coupled free/porous steady-state flows encountered in spontaneous ignition of porous coal stockpiles using mixed P2/P1 finite elements. The computations were observed to be totally insensitive to the values of slip coefficient employed at the interface which minimizes the effect of empiricism involved in the Beavers–Joseph slip condition. Gartling et al. [21] presented a finite element formulation to solve the coupled Navier–Stokes and Darcy system in context of two practical applications having a fixed free/porous interface and an emerging free/porous interface as in alloy solidification problems. The coupling of the Navier–Stokes and Darcy models exhibited the drawback of handling stress boundary conditions at the interface.

Discaccitati and Quarteroni [22] introduced a differential system based on the coupled Navier–Stokes/Darcy equations for the modelling of interactions between surface and groundwater flows. They proposed an iterative subdomian method based on a domain decomposition approach to solve the coupled flow problem using finite elements. At the free/porous boundary, the normal component of the Cauchy stress from the Stokes region is equated to the pressure from the Darcy domain. The tangential component of the Cauchy's stress is related to the seepage velocity in the porous region at the interface by a slip wall condition similar to Beavers and Joseph (1967) [44]. The significant contributions to this topic can be selectively listed as Mardal et al. [38] Miglio et al. [23] and Layton et al. [49].

The existence of viscous stress terms in the Navier–Stokes equations, which are in the form of second order PDEs makes straightforward linking of these equations to Darcy equations in a finite element scheme nearly impossible. To resolve this issue, Nassehi and Petera [39] presented a novel scheme for coupling Navier–Stokes and Darcy equations along a porous boundary in a flow regime representing an axisymmetric slurry filtration system. The scheme is based on least-squares finite element formulation in conjunction with use of C^1 continuous Hermite elements which avoid the formulation of inter-elemental flux terms and can be advantageously applied for combined flow problems without making any unrealistic assumptions. However these elements lack the inflexibility, in general and their application in complex domains is enormously complex and computationally expensive.

Later, Nassehi [24] developed a robust finite element simulation scheme for the combined Navier–Stokes/Darcy flows applicable for cross-flow filtration systems in which the imposed interfacial condition at the free/porous interface is the Darcy equation. A perturbed form of continuity equation is used, enhancing the employability of equal-order interpolation functions for velocity and pressure. The computational results using this scheme are found to preserve mass continuity in complex branching flow domains. The flexibility of this scheme was further analysed by subjecting variations in inlet fluid velocity, viscosity, porous wall permeability and exit conditions.

Damak et al. [25] reported an attempt to combine the Navier–Stokes and Darcy's equations to predict the growth of the concentration polarisation boundary layer in tubular cross-flow membrane filters. They simulated the fluid flow behaviour in a porous tube with variable wall suction. The flow throughout the free flow region is considered to be fully developed and variable wall suction is assumed along the length of the porous section. The governing equations are discretised using a finite difference numerical method. To simplify the model, the slip effect at the membrane surface is taken to be negligible as shown by Schmitz and Prat [26]. At the membrane surface, the axial velocity component and the radial velocity normal to the membrane surface have been expressed using the Darcy's equation. The simulations are carried out for a large range of Reynolds numbers with and without porous wall suctions. Although the results were theoretically validated through overall mass continuity checks the general assumption of the developed flow condition in these coupled flow regimes is still inappropriate and questionable.

More recently Rahimi et al. [27] carried out a CFD study to predict the water permeate flux through microfiltration membrane modules. They used time-averaged Navier–Stokes equations along with RNG version of the k–ε turbulent closure models to model flows within membrane cells. The source terms in the momentum balance Navier–Stokes equations were replaced by the Darcy equation in order to capture the effects of small scale turbulence. Finite

volume approach was adopted to discretise and solve the final system of equations in conjunction with use of a second order scheme and the SIMPLE pressure–velocity coupling algorithm. The simulations were carried out in large trapezoidal, small trapezoidal, skew barriers and empty cells through imposition of pressure boundary conditions at the inlet and outlets of the flow domain. Despite a robust 3D CFD modelling effort their model could not account for effects such as cake formation and appropriate treatment of flow hydrodynamics at the Navier–Stokes/Darcy interface which can result in significant errors in permeate flux measurements across the membrane barrier.

Zhang et al. [28] explored the use of CFD to implement a general gas–blood transport model for hollow fiber membrane-based oxygenators. The computational domain used in their studies consisted of an inlet, outlet, and a parallel flow chamber containing of a square fiber bed. The solid geometries were modelled in computer-aided design (CAD) software package Solidworks (Solidworks Corporation, Concord, MA, USA) and later meshed in Gambit (Fluent Inc., Lebanon, NH, USA) using 3D Tetrahedral/Hybrid elements. Porous flow hydrodynamics were approximated by the Ergun equation and in essence the porous media model is an added momentum sink in the Navier–Stokes momentum equations following a one-domain modelling approach. The blood oxygenation process was modelled using the convection–diffusion equation. An unstructured-mesh finite volume commercial CFD solver, Fluent (Fluent Inc., Lebanon, NH, USA), was used to solve the governing model equations in which user defined functions (UDF's) were written for the blood oxygenation process and coupled with Fluent. They validated their model against a mini-oxygenator available from Medtronic Affinity NT blood–gas oxygenator. However, intricacies arising from the treatment of flow hydrodynamics at the interfacial level were left ignored and are bound to result in errors for oxygenation mass transfer design predictions. Such intricacies left unresolved mainly through the use of general purpose commercial CFD codes based on one-domain approaches. Further, as they point out in their work, it still remains a challenging task to quantitatively analyse the local fluid dynamics to study the effects of packing of hollow fibers and structure of the membrane oxygenators on the oxygen transfer and blood trauma, because the blood flow pattern in membrane oxygenators is complicated and difficult to measure.

Chew et al. [29] developed an experimental technique known as Fluid Dynamic Gauging (FDG) to characterize the deposition of fouling layers on porous surfaces such as those experienced in membrane/filtration systems. They simulated, dead-end micro- and macro-filtration processes using filter paper and glass ballotini suspensions. FDG was then used to track, *in situ* and time-variant build-up of a ballotini cake during the filtration process. The permeate flux through the filter paper was also simultaneously monitored. The technique exploits the flow characteristics of the liquid as it is drawn by suction through the nozzle and knowledge of the flow rate of the fluid going through the nozzle will provide information on the nozzle location in space which can allow one to calculate the location of the surface, and thereby any change in the deposit layers, δ, resulting from deposition or cleaning can be determined from $\delta = h_0 - h$. To illustrate the flow hydrodynamics of FDG process they later performed CFD studies with particular focus on the flow patterns and stresses imposed on the porous surface. Governing equations comprising of Navier–Stokes, Darcy's and continuity equations were solved using the Augmented Lagrangian Finite Element Method implemented in a commercial partial differential equation solver, *Fastflo*™. The domain was represented using unstructured triangular elements and the governing equations were solved using a quadratic approximation. The code was initially used to solve a simple test case in a cross-flow filtration tubular membranes setup involving a laminar fluid flow along a porous pipe with variable wall suction. The flow was assumed to be axisymmetric, steady and incompressible and physical properties such as density, viscosity and porosity were assumed to be constant. The permeability of the filter paper was assumed to be homogenous and isotropic. The feed stream in the pipe tangential to the porous wall was modelled using the Navier–Stokes equation whilst the variable suction at the porous wall was described by Darcy's law. An interesting aspect of all their CFD simulations was the approximation of interface free/porous boundary as a surface of the filter paper in which the axial velocity at the permeable surface was given by the Darcy's law and the slip velocity was assumed to be zero. They claimed that the slip effect at the permeable surface in a cross-flow filtration system is practically negligible and thus imposed the no-slip boundary condition at the interface. However, it has been previously shown by Reddy and Gartling [30] that imposition of no-slip wall boundary conditions at the free/porous interface is incompatible with the solution of Darcy equation.

It is apparent from most of the recent studies in the literature that modelling of coupled free/porous flows is based on many simplifying assumptions. Some of the researchers consider the use of Brinkman equation to safely avoid the incompatibility constraints posed by the mathematical operators whilst others have developed models which are only applicable to simplistic geometric domains with reasonably high permeability, and thus their applications to real life engineering problems is still restrictive.

The current work is a subsidiary effort realised through a multidisciplinary EU project focusing on hydrodynamic modelling of dead-end filtration systems that are used for actuation of hydraulic lubrication systems in commercial airliners. Taking into consideration the wide scale industrial applicability of the filtration processes, initially a two-dimensional model was developed for simulating dead-end filtration processes, which was later extended to cater the needs of cross-flow membrane filtration industry. The present work can also be regarded as an advanced version of the works previously carried out by Nassehi [24].

In this work, the governing equations of the cross-flow filtration setup are solved using the finite element method in conjunction with the use of mixed P2/P1 C^0-continuous rectangular elemental approximations for velocity and pressure fields in order to satisfy the Ladyhenskaya Babuska Brezzi (LBB) stability criterion [31,32] for incompressible flow problems. Reviewing the discussion of interface conditions, it can be inferred that the imposition of artificial interface conditions become impracticable for special cases of combined flow problems encountered in industrial filtration processes. Therefore in the current work the free and porous flow equations have been linked at the interface using a nodal replacement procedure developed by Nassehi et al. [33], Hanspal et al. [34,36] and Wakeman et al. [41].

The free flow is modelled by the Stokes equations for the creeping flow regime whereas the porous flow dynamics is represented by the Darcy equation. The developed model is capable of simulating both Newtonian and non-Newtonian fluid flows. The interface separating the free and porous flow regimes is considered to be curved surface, which is the case in cross-flow filtration. A series of numerical experiments are carried out to examine the robustness and compatibility of the developed scheme for permeability values ranging between 10^{-6} and 10^{-12} m^2 for variant operating conditions. The developed computer code has also been analysed for complex geometrical computational domains usually observed in filtration equipments. The converged results from our simulations have been theoretically validated for their accuracy by evaluating mass balance continuity across the computational domains. The developed simulation software will provide supportive evidence for the validity of any experimental data but will not replace any of the pure theoretical concepts related to an actual process.

2. Mathematical model

A two-dimensional mathematical model, based on flow and constitutive equations is considered. The domains consist of a free flow region described by the Stokes equations and the porous region described by the Darcy equation. In the absence of body forces the creeping, steady-state, isothermal flow of a shear thickening (STF) generalised Newtonian fluid in coupled free/porous regimes can be represented by the following equations.

Conservation of momentum:

(a) Free flow regime

$$\begin{cases} -\dfrac{\partial p}{\partial x} + \dfrac{\partial}{\partial x}\left[2\eta\dfrac{\partial v_x}{\partial x}\right] + \dfrac{\partial}{\partial y}\left[\eta\left(\dfrac{\partial v_x}{\partial y} + \dfrac{\partial v_y}{\partial x}\right)\right] = 0 \\ -\dfrac{\partial p}{\partial y} + \dfrac{\partial}{\partial y}\left[2\eta\dfrac{\partial v_y}{\partial y}\right] + \dfrac{\partial}{\partial x}\left[\eta\left(\dfrac{\partial v_y}{\partial x} + \dfrac{\partial v_x}{\partial y}\right)\right] = 0 \end{cases} \quad (1)$$

where, p is the pressure, v_x and v_y are the fluid velocity in x- and y-directions respectively and η is the fluid viscosity.

(b) Porous flow regime

$$\begin{aligned} \frac{\eta}{K_x}v_x + \frac{\partial p}{\partial x} = 0 \\ \frac{\eta}{K_y}v_y + \frac{\partial p}{\partial y} = 0 \end{aligned} \quad (2)$$

Equation of continuity:

$$\frac{\partial v_x}{\partial x} + \frac{\partial v_y}{\partial y} = 0 \quad (3)$$

2.1. Boundary conditions

The governing equations are solved subject to the following boundary conditions. At the inlet of the free flow region a plug flow velocity is specified. On the impermeable boundaries of the free flow region, no-slip wall velocity boundary conditions are imposed, whilst on the permeable boundaries of the porous region perfect slip wall boundary conditions are imposed. At the free/porous interface no artificial condition is imposed, instead a direct linking procedure has been employed. Finally at the exit of the porous domain a zero pressure datum has been imposed. At the exit of the free flow domain stress-free boundary conditions (in essence no boundary conditions) have been imposed. This is automatically achieved by neglecting the line integrals in the finite element working equations (refer [33] for details) of combined flow model.

2.2. Finite element formulations

The finite element method employed in the present work is based on the UVP scheme in which all the field variables, i.e. velocity components and pressures, are calculated simultaneously. The unknown variables u, v and p are approximated over an element as:

$$u \approx \tilde{u} = \sum_{j=1}^{n} N_j u_j; \quad v \approx \tilde{v} = \sum_{j=1}^{n} N_j v_j; \quad p \approx \tilde{p} = \sum_{l=1}^{m} M_l p_l$$

where, N_j and M_l are the velocity and pressure shape functions respectively ($m < n$).

After substitution of these approximations into the governing equations and weighting of the generated residuals via the standard Galerkin method, the weak variational formulation corresponding to the combined free/porous flow model is obtained. To reduce the inter-element continuity requirement of field variables to C^0 the second order differentials of velocity, and to maintain the consistency of the formulation of the first order differentials of pressure in this statement, are treated by Green's theorem respectively. Line integrals appearing after the application of Green's theorem are taken to the right hand side of the variational statement [50]. These line integrals cancel out during the final assembly of the stiffness matrices or are replaced using the boundary conditions. The final finite element working equations for the coupled free/porous flow model can be obtained from Nassehi et al. [33].

To couple the two different flow regimes, the Darcy equation is imposed effectively as the boundary condition for the Stokes equation at the free/porous interface. This imposition alleviates the complex situation of matching the flux terms (i.e. line integrals) arising in both the domains. In the stiffness matrix of the free flow elements present on the free/porous interface, the Stokes terms corresponding to the interfacial nodes are replaced by the appropriate form of the discretised Darcy components, and vice versa at the porous/free interface. The complete procedure for the numerical linking of the coupled flow regime can be elaborated with the help of Fig. 1.

Fig. 1 shows the three elements in the Stokes flow region P, X and Q connected in series in the direction of flow. The element X is connected at the bottom to the element Y which is in the Darcy flow region. The overall assembly replicates the situation that occurs in a typical cross-flow filtration process. The boundary AB of the Stokes element X coincides with boundary A′B′ of the Darcy element Y at the free/porous interface. Here, i_1, j_1 and k_1 are the nodes of the Stokes element X on the free/porous interface AB–A′B′ whereas i_2, j_2 and k_2 are the interfacial nodes for the Darcy element Y. In the final assembly of stiffness matrices, terms corresponding to nodes i_1, j_1 and k_1 of the Stokes element X are replaced by the terms corresponding to nodes i_2, j_2 and k_2 of the Darcy element Y. This substitution circumvents the difficulty arising from imposing any artificial boundary conditions on the free/porous interface without violating the physics behind the coupled flow phenomenon.

3. Results and discussion

Results presented in this manuscript have been simulated using the extended version of an FEM based in-house code named **ACFAMP** (Ph.D. Thesis: [33,34]) Aircraft Cartridge Filter Analysis Filter Modelling Program written in FORTRAN. This code has been used for modelling combined flows in dead-end and cross-flow filtration applications. Results have been presented for two identical rectangular channel domains with distinct interfacial boundary separating the free and porous flow regions. In all the computations, the fluid is considered to be a generalised Newtonian fluid with a power law index of 1.0. The consistency coefficient in the power law model is taken to be 80 Pa s and the density of fluid is assumed to be 970 kg m^{-3}. The porous matrix is assumed to be homogeneous and isotropic. For both the computational domains, simulations are carried out for permeability values ranging between 10^{-6} and 10^{-12} m^2. Results are presented for two extreme values of permeability, i.e. 10^{-6} and 10^{-12} m^2.

In the first case, a rectangular cross-flow membrane filtration module is considered with a flat free/porous interface as shown in Fig. 2 with all the imposed boundary conditions.

The length of the free flow domain is 0.015 m with a width of 0.005 m. The length of the porous region is 0.0075 m with a width of 0.0025 m. The overall width of the domain extending in the radial direction is 0.005 m. The height of the rectangular exit is small compared to that of the inlet and is 0.00125 m.

The overall domain is discretised with 9-noded Lagrangian Taylor-Hood elements. The total number of elements is 2000 which corresponds to 8221 nodes. In the context of these boundary condi-

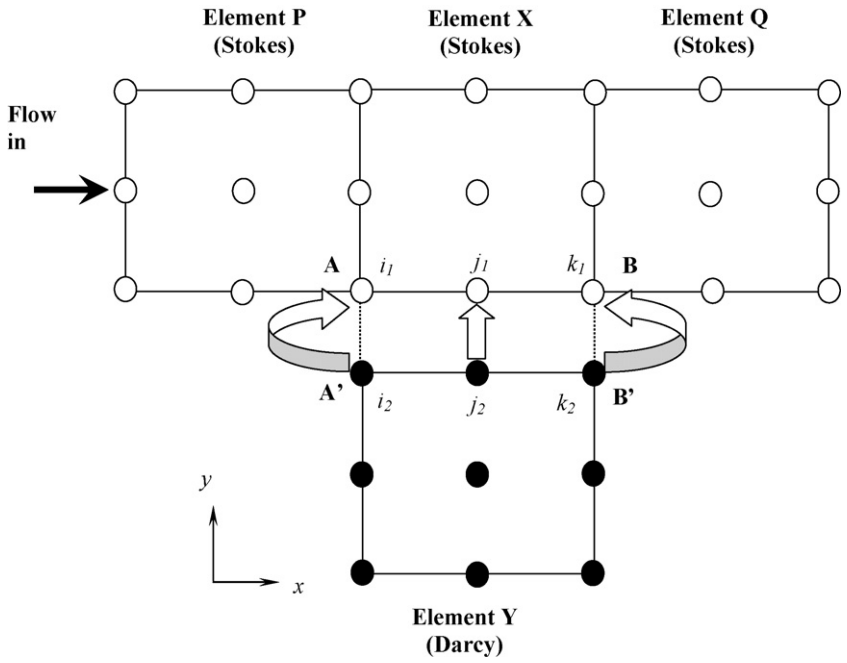

Fig. 1. Schematic representation of linking of stokes and darcy regimes.

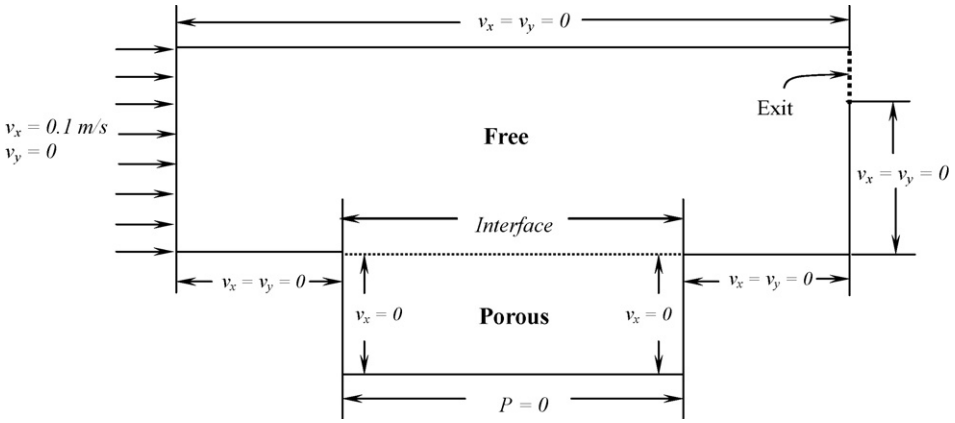

Fig. 2. Boundary conditions on the rectangular cross-flow filtration domain with flat free/porous interface.

tions, simulations are carried out for two values of permeability of the porous medium. When the permeability of the porous medium is 10^{-6} m^{-2}, the simulated flow field developed is pictorially represented in the form of velocity vectors in Fig. 3.

As the permeability of the porous medium is very high, most of the fluid entering the domain seeps across the free/porous interface to the bulk of the porous medium. A very small amount finds its way through the exit of the rectangular free flow channel and as a result

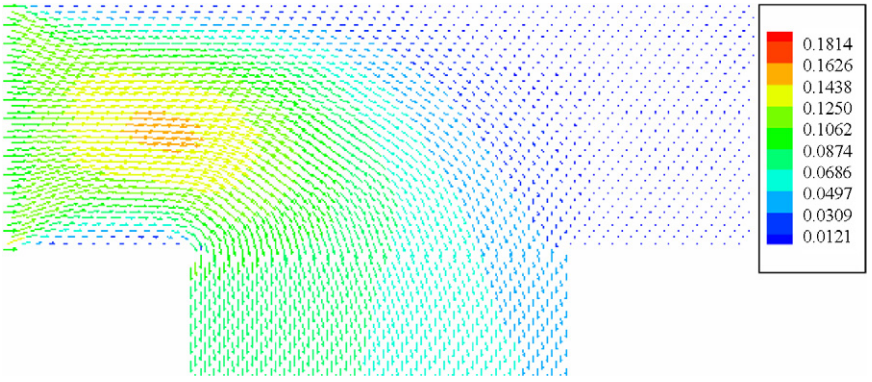

Fig. 3. Developed flow filed over the rectangular cross-flow filtration domain with flat free/porous interface with permeability of porous medium 10^{-6} m^2.

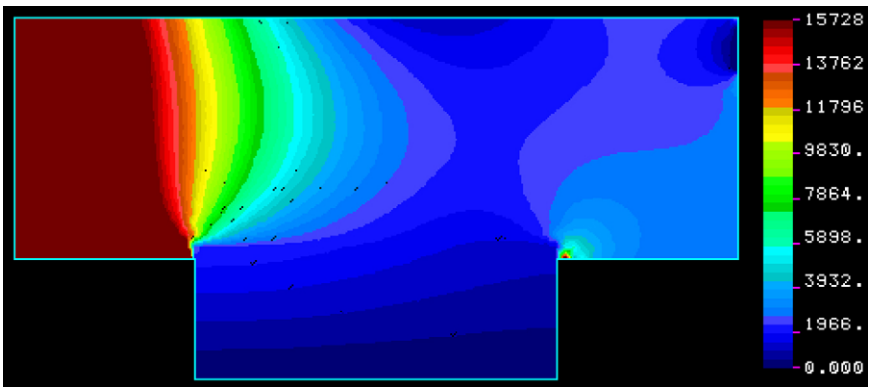

Fig. 4. Developed pressure field over the rectangular cross-flow filtration domain with flat free/porous interface with permeability of porous medium 10^{-6} m^2.

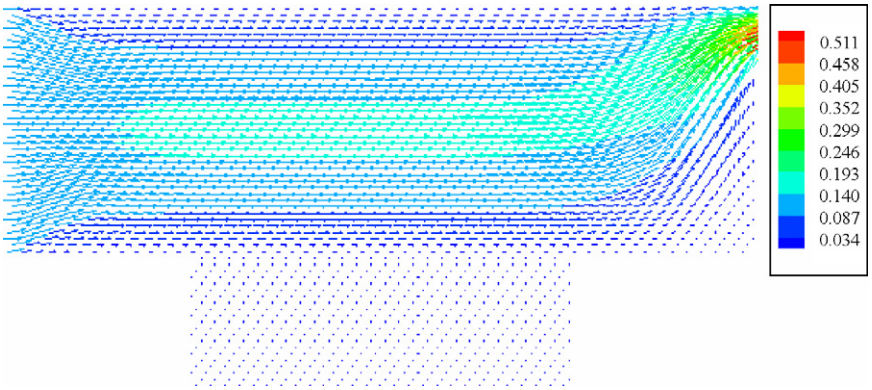

Fig. 5. Developed flow field over the fectangular cross-flow filtration domain with flat free/porous interface with permeability of porous medium 10^{-12} m^2.

a dead-zone is observed in the bottom right corner in the free flow channel Ω_f. The flow tends to attain a developed parabolic state before entering the porous matrix. At every computational point in the porous regime, the flow is in plug flow state. The developed pressure field over the entire computational domain is represented in the form of coloured contours in Fig. 4.

The pressure values in the free flow channel are relatively constant before the fluid reaches the free/porous barrier. As the fluid penetrates across the interface, a pressure gradient is observed being developed in the direction of flow. In the porous matrix, a gradual decrease in pressure values is observed as the fluid seeps through the pores. A localised low-pressure region is observed in the vicinity of the narrow exit of the free flow region.

In the second experiment, the permeability of the porous medium is lowered to the value of 10^{-12} m^2. The simulated velocity vectors of this coupled flow system are represented in Fig. 5.

Although, the inlet fluid is in uniform plug flow condition, it shows the tendency to attain a fully developed parabolic profile in the free flow region. Since the permeability of the porous matrix is very low, a small amount of fluid is observed to be successful in penetrating the free/porous interface. All the fluid is observed to get concentrated near the narrow exit and a localised high velocity field is observed in that region. The amount of fluid flowing through the porous matrix can be found by calculating the mass balance over the domain. It is found that only 1.5% of the inlet fluid is passing through the porous barrier and the rest about 98.5% is flowing across the free flow region. The discrepancy between the inlet and outlet masses amounts to 3%, which is within a satisfactory limit and primarily can be attributed to mesh refinement.

The corresponding hydrostatic pressure field is shown in Fig. 6 in the form of flooded contours.

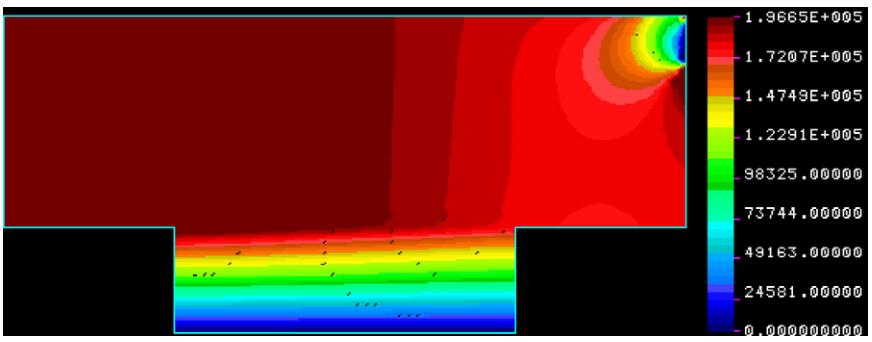

Fig. 6. Developed pressure field over the rectangular cross-flow filtration domain with flat free/porous interface with permeability of porous medium 10^{-12} m^2.

Table 1
Mass balance calculations for rectangular domain with straight free/porous interface.

Permeability (m^2)	Total mass in (M_{in}) (kg)	Mass at exit (E_{mass}) (kg)	Mass of permeate (P_{mass}) (kg)	Total mass out (M_{out}) = E_{mass} + P_{mass} (kg)	%Error = $\frac{M_{in}-M_{out}}{M_{in}} \times 100$
1×10^{-6}	4.7894×10^{-4}	5.6371×10^{-6}	4.7511×10^{-4}	4.8075×10^{-4}	−0.3789
1×10^{-7}	4.7894×10^{-4}	3.1740×10^{-5}	4.4802×10^{-4}	4.7976×10^{-4}	−0.1727
1×10^{-8}	4.7894×10^{-4}	1.9286×10^{-4}	2.8079×10^{-4}	4.7364×10^{-4}	1.1051
1×10^{-9}	4.7894×10^{-4}	4.0502×10^{-4}	6.0549×10^{-5}	4.6556×10^{-4}	2.7915
1×10^{-10}	4.7894×10^{-4}	4.5659×10^{-4}	7.0103×10^{-6}	4.6360×10^{-4}	3.2019
1×10^{-11}	4.7894×10^{-4}	4.6266×10^{-4}	7.1374×10^{-7}	4.6338×10^{-4}	3.2486
1×10^{-12}	4.7894×10^{-4}	4.6328×10^{-4}	7.1125×10^{-8}	4.6335×10^{-4}	3.2538

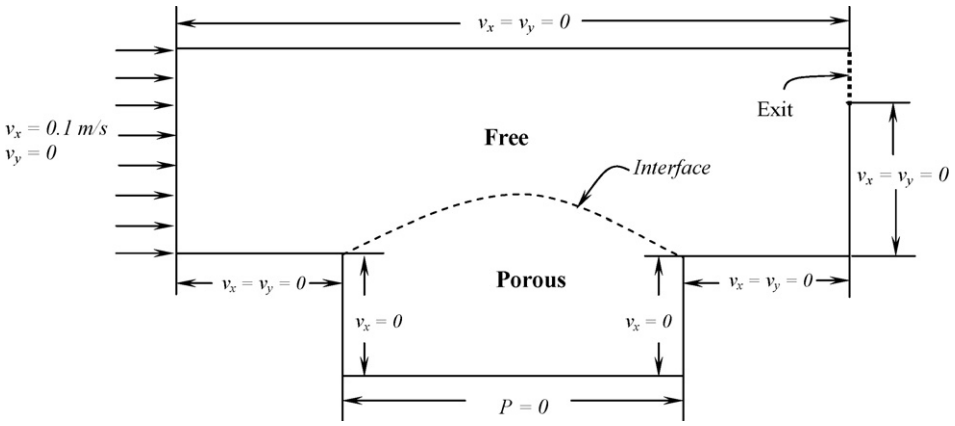

Fig. 7. Boundary conditions on the rectangular cross-flow filtration domain with curved free/porous interface.

The pressure in the free flow region is changing as the fluid passes through the porous region. In the porous region, a steep gradient in pressure is observed. Due to the stress-free boundary condition at the exit, a low-pressure field is observed there.

For all the simulations, the validity of the developed model has been examined by means of a mass balance calculated over the entire computational domain. All the mass balance figures are listed in Table 1 against the corresponding permeability values.

The mass of fluid permeating the porous media decreases as the permeability of the porous matrix decreases.

The second domain is identical to the one discussed previously except that the interface separating the free and porous regimes is curved, convex towards the free flow region as shown in Fig. 7. The coupled free/porous flow domain with the curved interface is a common feature of numerous cross-flow filtration equipments.

Due to continuous deposition of particles at the interface during filter operation, the flat interface may become a curved one (although the precise nature of the curvature is not known).

The overall domain is tessellated with 9-noded Lagrangian Taylor-Hood elements. The total number of nodes is 8221 corresponding to 2000 elements. Similar to the case with the previous domain, numerical experiments were carried out for two different permeability values of the porous medium. For the implied boundary conditions, the simulated velocity field over the domain with the permeability of the porous medium of the value of 10^{-6} m^{-2} is shown by velocity vectors in Fig. 8.

Due to the high permeability of the porous regime, the free/porous interface does not pose any severe obstruction for the fluid to enter the bulk of the porous medium. Therefore, most of the fluid inlet to the rectangular channel finds its way through the porous matrix, crossing the free/porous barrier. A very small amount of fluid is successful in reaching the narrow exit of the free flow channel.

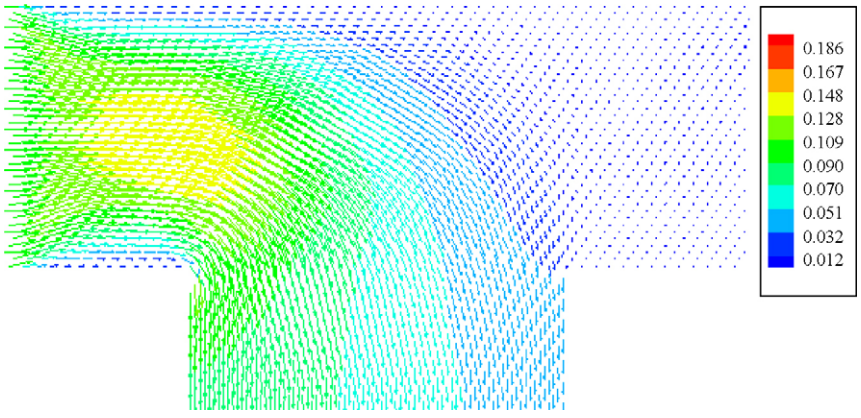

Fig. 8. Developed flow field over the rectangular cross-flow filtration domain with curved free/porous interface with permeability of porous medium 10^{-6} m^2.

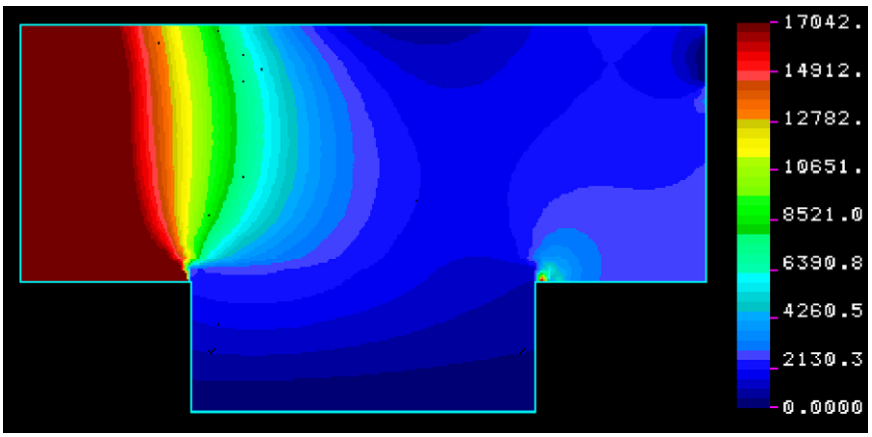

Fig. 9. Developed pressure field over the rectangular cross-flow filtration domain with curved free/porous interface with permeability of porous medium 10^{-6} m^2.

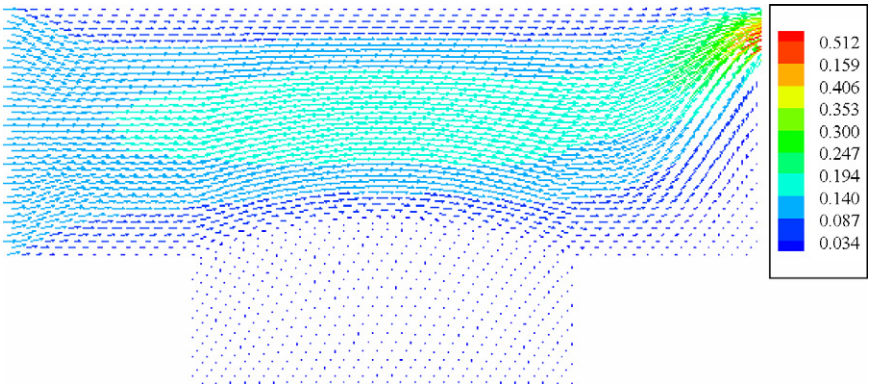

Fig. 10. Developed flow field over the rectangular cross-flow filtration domain with curved free/porous interface with permeability of porous medium 10^{-12} m^2.

The developed pressure field distribution over the entire computational domain can be analysed with the help of pressure contours in Fig. 9.

The pressure values in the free flow channel are relatively constant before the fluid reaches the free/porous barrier. As the fluid penetrates across the interface, a steep pressure gradient is developed in the free flow channel. In the porous matrix, a gradual decrease in pressure values is observed as the fluid seeps through the pores. A localised low-pressure region is observed in the vicinity of the narrow exit of the free flow region. A small high pressure region is observed at the right hand side corner of the free/porous interface, designating it as a singular point in the mathematical sense.

Similar to the case with the flat interface, the permeability of the porous medium is lowered to the value of 10^{-12} m^2 and the simulated flow field over the domain is represented in the form of velocity vectors in Fig. 10.

The developed flow field over this coupled domain with a curved free/porous interface is similar to that in the domain with flat interface. As the permeability of the porous medium is very low, the free/porous interface presents a stringent barrier for the fluid to enter the bulk of the porous matrix. Therefore, a very small amount of the inlet fluid seeps through the porous medium and most of the fluid slides across the curved interface and flows towards the narrow exit of the rectangular free flow channel. A high velocity region is observed in the vicinity of the exit due to the reduced

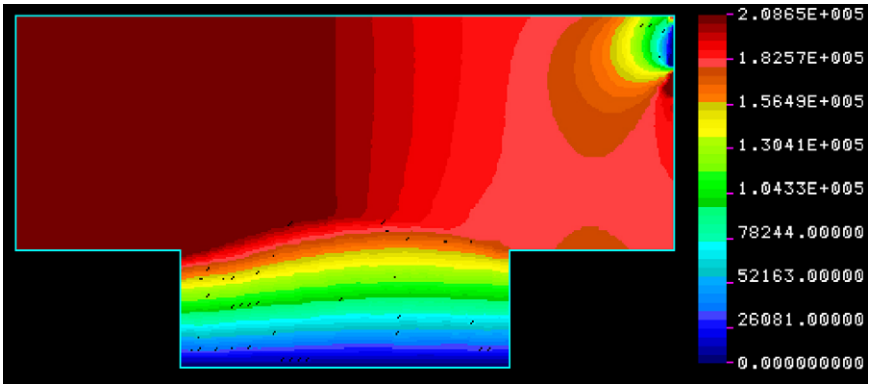

Fig. 11. Developed pressure field over the rectangular cross-flow filtration domain with curved free/porous interface with permeability of porous medium 10^{-12} m^2.

Table 2
Mass balance calculations for the rectangular domain with curved free/porous interface.

Permeability (m^2)	Total mass in (M_{in}) (kg) ($\times 10^4$)	Mass at exit (E_{mass}) (kg) ($\times 10^4$)	Mass of permeate (P_{mass}) (kg)	Total mass out (M_{out}) = E_{mass} + P_{mass} (kg) ($\times 10^4$)	%Error = $\frac{M_{in}-M_{out}}{M_{in}} \times 100$
1×10^{-6}	4.7894	0.0487	5.0820×10^{-4}	5.1307	−7.126
1×10^{-7}	4.7894	0.3323	4.7687×10^{-4}	5.1010	−6.505
1×10^{-8}	4.7894	2.0603	2.8612×10^{-4}	4.9215	−2.756
1×10^{-9}	4.7894	4.1286	5.7889×10^{-5}	4.7075	1.710
1×10^{-10}	4.7894	4.5937	6.5782×10^{-6}	4.6595	2.712
1×10^{-11}	4.7894	4.6470	6.6805×10^{-7}	4.6536	2.827
1×10^{-12}	4.7894	4.6528	6.6673×10^{-8}	4.6335	2.839

cross-section of the exit port resulting in higher flow rate. The mass balance is checked over the domain calculating the discrepancy between the inlet and outlet mass of the fluid, which is about 3%. The amount of fluid passing through the porous barrier is just 1.4% and most of the fluid finds its way through the exit of the free flow domain.

The hydrostatic pressure field over the domain due to incompressible flow of a Newtonian fluid is shown in Fig. 11.

Before the porous barrier, the pressure in the free flow region is almost constant. As the fluid approaches the free/porous interface, the pressure in the free flow region goes down since some of the fluid is penetrating the porous medium. In the porous regime, the pressure gradually decreases and attains a null value at the exit of the permeate zone. A localised low-pressure vortex is observed at the exit of free flow region, where most of the fluid is pushed through the narrow outlet.

Similar to the previous domain, the validity of the model is tested by quantitative evaluations based on overall mass balance calculations. The mass inflows and outflows figures for a range of permeability values are tabulated in Table 2,

In the present case, the discrepancy between inlet and outlet masses is also found to be increasing as the porous medium becomes less permeable. A possible solution to minimize this discrepancy may be accomplished by refining the computational mesh.

4. Conclusions

A finite element model for the solution of flow equations in a two-dimensional coupled domain has been developed, where one-domain is a free flow region and the other is a porous material. Sample results for two geometries of differing complexity have been presented which indicate the robustness of the scheme. All the simulations were carried out for a wide range of permeability values of the porous medium, lying between 10^{-6} and 10^{-12} m^2. At very high permeability values, the discrepancy in mass balance calculations is observed to be significant. When the permeability is reduced the model has to cope with smaller numbers and hence a higher precision is required. Similarly when domain with curved boundaries is modelled a higher precision is required. Considering the trend of the mass balance error in the present work such conclusions are confirmed. In all cases we therefore, expect to reduce such errors by mesh refinement. At a low permeability, a very small amount of fluid succeeds in crossing the free/porous barrier and most of the fluid leaves the domain through the free flow exit. In the free flow region, the flow is fully developed before it starts entering into the porous region. The geometry of the free/porous interface is observed to affect the amount of fluid passing through the porous medium as permeate. The model has been theoretically validated by calculating the mass balance over the domains. The discrepancy in the balance in both the domains lies within an acceptable limit of about 3%. The finite elements with unequal order interpolation functions for velocity and pressure generates stable and accurate solutions. When this coupled flow model is incorporated into a particle transport model, it will provide a robust and cost-effective design and analysis tools for predicting the hydrodynamics in industrial cross-flow filtration processes.

Acknowledgement

The authors wish to acknowledge financial support provided by the European Commission Contract No. GARD-CT-2001-00609 which made this work possible.

References

[1] G. Belfort, N. Nagata, Fluid mechanics and cross-flow filtration: some thoughts, Desalination 53 (1985) 57–59.
[2] G. Belfort, Fluid mechanics in membrane filtration: recent developments, Journal of Membrane Science 40 (1989) 123–147.
[3] R.P. Ma, C.H. Gooding, W.K. Alexander, A dynamic model for low-pressure, hollow fiber ultrafiltration, AIChE Journal 31 (10) (1985) 1728–1732.
[4] L. Song, M. Elimelech, Particle deposition onto a permeable surface in laminar flow, Journal of Colloid and Interface Science 173 (1995) 165–180.
[5] L. Huang, M.T. Morrissey, Finite element analysis as a tool for crossflow membrane filter simulation, Journal of Membrane Science 155 (1999) 19–30.
[6] S. Ripperger, J. Altmann, Crossflow simulation—state of the art, Separation and Purification Technology 26 (2002) 19–31.
[7] A.S. Berman, Laminar flow in channels with porous walls, Journal of Applied Physics 24 (9) (1953) 1232–1235.
[8] R.M. Terril, P.W. Thomas, On laminar flow through a uniformly porous pipe, Applied Science Research 21 (1969) 37–53.
[9] J.P. Quaile, E.K. Levy, Laminar flow in a porous tube with suction, Journal of Heat Transfer 2 (1975) 66–71.
[10] L. Oxarango, P. Schmitz, M. Quintard, Laminar flow in channels with wall suction or injection: a new model to study multi-channel filtration systems, Chemical Engineering Science 59 (5) (2004) 1039–1051.
[11] D.A. Nield, A. Bejan, Convection in Porous Media, 1st edition, Springer-Verlag, London, 1992.
[12] S. Kim, W.B. Russell, Modelling of porous media by renormalization of the Stoke's equations, Journal of Fluid Mechanics 154 (1985) 269–286.
[13] L. Durlofski, J.F. Brady, Analysis of the Brinkman equation as a model for flow in porous media, Physics of Fluids 30 (1987) 3329–3341.
[14] C.T. Hsu, P. Cheng, The Brinkman model for natural convection about a semi-infinite vertical flat plate in porous medium, International Journal of Heat and Mass Transfer 28 (3) (1985) 683–697.
[15] K. Vafai, R. Thiyagaraja, Analysis of flow and heat transfer at the interface region of a porous medium, International Journal of Heat and Mass Transfer 30 (1987) 1391–1405.
[16] I.P. Jones, Low Reynolds Number Flow Past a Porous Spherical Shell, in: Proceedings of the Cambridge Philosophical Society, vol. 73, 1973, pp. 231–238.
[17] G. Neale, W. Nader, Practical significance of Brinkman's extension of Darcy's Law: coupled parallel flows within a channel and a bounding porous medium, Canadian Journal of Chemical Engineering 52 (1974) 475–478.
[18] M. Sahraoui, M. Kaviany, Slip and no-slip velocity boundary conditions at the interface of porous plain media, International Journal of Heat and Mass Transfer 35 (4) (1992) 927–933.
[19] (a) J. A. Ochoa-Tapia, S. Whitaker, Momentum transfer at the boundary between a porous medium and a homogeneous fluid–I. Theoretical development, International Journal of Heat and Mass Transfer, Volume 38, Issue 14, September 1995a, Pages 2635-2646, ISSN 0017-9310, doi:10.1016/0017-9310(94)00346-W.;
(b) J. A. Ochoa-Tapia, S. Whitaker, Momentum transfer at the boundary between a porous medium and a homogeneous fluid–II. Comparison with experiment, International Journal of Heat and Mass Transfer, Volume 38, Issue 14, September 1995, Pages 2647-2655, ISSN 0017-9310, doi:10.1016/0017-9310(94)00347-X.
[20] A.G. Salinger, R. Aris, J.J. Derby, Finite element formulations for large-scale, coupled flows in adjacent porous and open fluid domains, International Journal for Numerical Methods in Fluids 18 (12) (1994) 1185–1209.

[21] D.K. Gartling, C.E. Hickox, R.C. Givler, Simulation of coupled viscous and porous flow Problems, Computational Fluid Dynamics 7 (1996) 23–48.
[22] M. Discacciati, A. Quarteroni, Analysis of domain decomposition method for the coupling of Stokes and Darcy equations, in: F. Brezzi, S. Buffa, S. Corsaro, A. Murali (Eds.), Numerical Mathematics and Advanced Applications—ENUMATH 2001, Springer, Milan, Italy, 2003, pp. 3–20.
[23] E. Miglio, A. Quarteroni, F. Saleri, Coupling of free surface and groundwater flows, Computers for Fluids 32 (1) (2003) 73–83.
[24] V. Nassehi, Modelling of combined Navier–Stokes and Darcy flows in crossflow membrane filtration, Chemical Engineering Science 53 (6) (1998) 1253–1265.
[25] (a) K. Damak, A. Ayadi, P. Schmitz, B. Zeghmati, Modeling of crossflow membrane separation processes under laminar flow conditions in tubular membrane, Desalination, Volume 168, Desalination Strategies in South Mediterranean Countries, 15 August 2004a, Pages 231-239, ISSN 0011-9164, DOI:10.1016/j.desal.2004.07.003.;
(b) K. Damak, A. Ayadi, B. Zeghmati, P. Schmitz, A new Navier-Stokes and Darcy's law combined model for fluid flow in crossflow filtration tubular membranes, Desalination, Volume 161, Issue 1, 5 February 2004b, Pages 67-77, ISSN 0011-9164, DOI:10.1016/S0011-9164(04)90041-0.
[26] P. Schmitz, M. Prat, 3D laminar stationary flow over a porous surface with suction: description at pore level, AIChE Journal 41 (10) (1995) 2212–2226.
[27] M. Rahimi, S.S. Madaeni, K. Abbasi, CFD modeling of permeate flux in cross-flow microfiltration membrane, Journal of Membrane Science 255 (1) (2005) 23–31.
[28] J. Zhang, T.D.C. Nolan, T. Zhang, B.P. Griffith, Z.J. Wu, Characterization of membrane blood oxygenation devices using computational fluid dynamics, Journal of Membrane Science 288 (1) (2007) 268–279.
[29] Y.M.J. Chew, W.R. Paterson, D.I. Wilson, Fluid dynamic gauging: a new tool to study deposition on porous surfaces, Journal of Membrane Science 296 (1) (2007) 29–41.
[30] J.N. Reddy, D.K. Gartling, The Finite Element Method in Heat Transfer and Fluid Dynamics, 2nd edition, CRC Press Ltd., London, 1994.
[31] J.N. Reddy, An Introduction to the Finite Element Method, 2nd edition, McGraw-Hill, New York, 1993.
[32] J. Donea, A. Huerta, Finite Element Methods for Flow Problems, Wiley-VCH, New York, 2003 (ISBN-10:0-471-49666-9).
[33] V. Nassehi, N.S. Hanspal, A.N. Waghode, W.R. Ruziwa, R.J. Wakeman, Finite element simulation of flow through pleated cartridge filters, Chemical Engineering Science 60 (4) (2005) 995–1006.
[34] Hanspal, N.S., 2005. Finite element modelling of high performance aeronautical filters, Ph.D. Thesis, Department of Chemical Engineering, Loughborough University, UK.
[35] S.G. Chatterjee, G. Belfort, Fluid flow in idealised spiral wound membrane module, Journal of Membrane Science 28 (1986) 191–200.
[36] N.S. Hanspal, A.N. Waghode, V. Nassehi, R.J. Wakeman, Numerical analysis of coupled Stokes/Darcy flows in industrial filtrations, Transport in Porous Media 74 (1) (2005) 73–103.
[37] J.L. Lage, in: D.B Ingham, I. Pop (Eds.), The Fundamental Theory of Flow Through Permeable Media from Darcy to Turbulence in Transport Phenomena in Porous Media, Elsevier Science Limited, Oxford, Pergamon, 1998, pp. 1–30.
[38] K.A. Mardal, X. Tai, R. Winther, A robust finite element method for Darcy–Stokes flow, SIAM Journal on Numerical Analysis 40 (5) (2002) 1605–1631.
[39] V. Nassehi, J. Petera, A new least-square finite element model for combined Navier–Stokes and Darcy flows in geometrically complicated domains with solid and porous boundaries, International Journal for Numerical Methods in Engineering 37 (1994) 1609–1620.
[40] P. Schmitz, D. Houi, Wandelt, Hydrodynamic aspects of crossflow microfiltration: analysis of particle deposition at the membrane surface, Journal of Membrane Science 71 (1992) 29–40.
[41] R.J. Wakeman, N.S. Hanspal, A.N. Waghode, V. Nassehi, Analysis of pleat crowding and medium compression in pleated cartridge filters, Chemical Engineering Research and Design 83 (10) (2005) 1246–1255.
[42] C. J. Richardson, V. Nassehi, Finite element modelling of concentration profiles in flow domains with curved porous boundaries, Chemical Engineering Science, Volume 58, Issue 12, June 2003, Pages 2491-2503, ISSN 0009-2509, DOI:10.1016/S0009-2509(03)00118-0.
[43] S.W. Yuan, A.B. Finkelstein, Laminar Flow with Injection and Suction Through a Porous Wall, Trans. ASME 78 (1956) 719–724.
[44] G.S. Beavers, D.D. Joseph, Boundary conditions at the natural permeable wall, Journal of Fluid Mechanics 30 (Part 1) (1967) 197–207.
[45] H.C. Brinkman, A calculation of the viscous force exerted by a flowing fluid on a dense array of particles, Applied Scientific Research A1 (1947) 27–34.
[46] T.S. Lundgren, Slow flow through stationary random beds and suspensions of spheres, J. Fluid Mech. 51 (1972) 273–299.
[47] P.G. Saffman, On the boundary condition at the surface of a porous medium, Studies in Applied Mathematics 1 (1971) 93–101.
[48] S. Haber, R. Mauri, Boundary conditions for Darcy's flow through porous medium, Int. J. Multiphase Flow 9 (5) (1983) 561–574.
[49] W.J. Layton, F. Schieweck, I. Yotov, Coupling fluid flow with porous media flow, SIAM Journal of Numerical Analysis 40 (6) (1993) 2195–2218.
[50] O.C. Zienkiewicz, R.L. Taylor, The Finite Element Method, vol.3, fifth ed., Butterworth-Heinemann, Oxford, 2002.